J Biol Inorg Chem (2002) 7: 461–472
DOI 10.1007/s00775-001-0321-3

ORIGINAL ARTICLE

**Mikhail L. Antonkine · Gaohua Liu · Detlef Bentrop
Donald A. Bryant · Ivano Bertini · Claudio Luchinat
John H. Golbeck · Dietmar Stehlik**

Solution structure of the unbound, oxidized Photosystem I subunit PsaC, containing [4Fe-4S] clusters F_A and F_B: a conformational change occurs upon binding to Photosystem I

Received: 29 June 2001 / Accepted: 29 October 2001 / Published online: 11 January 2002

Abstract This work presents the three-dimensional NMR solution structure of recombinant, oxidized, unbound PsaC from *Synechococcus* sp. PCC 7002. Constraints are derived from homo- and heteronuclear one-, two- and three-dimensional ^{1}H and ^{15}N NMR data. Significant differences are outlined between the unbound PsaC structure presented here and the available X-ray structure of bound PsaC as an integral part of the whole cyanobacterial PS I complex. These differences mainly concern the arrangement of the N- and C-termini with respect to the [4Fe-4S] core domain. In the NMR solution structure of PsaC the C-terminal region assumes a disordered helical conformation, and is clearly different from the extended coil conformation, which is one of the structural elements required to anchor PsaC to the PS I core heterodimer. In solution the N-terminus of PsaC is in contact with the pre-C-terminal region but slides in between the latter and the iron-sulfur core region of the protein. Together, these features result in a concerted movement of the N-terminus and pre-C-terminal region away from the F_A binding site, accompanied by a bending of the N-terminus. In comparison, the same terminal regions are positioned much closer to F_A and take up an anti-parallel β-sheet arrangement in PsaC bound to PS I. The conformational changes between bound and unbound PsaC correlate with the differences reported earlier for the EPR spectra of reduced F_A and F_B in bound versus unbound PsaC. The observed different structural features in solution are highly relevant for unraveling the stepwise assembly process of the stromal PsaC, PsaD and PsaE subunits to the PS I core heterodimer. Electronic supplementary material to this paper can be obtained by using the Springer Link server located at http://dx.doi.org/10.1007/s00775-001-0321-3.

Keywords Nuclear magnetic resonance · Solution structure · Iron-sulfur protein · Photosystem I

Abbreviations *PS I*: Photosystem I · *F_A and F_B*: the two [4Fe-4S] clusters of PsaC in PS I · *F_X*: interpolypeptide iron-sulfur cluster in PS I · *HSQC*: heteronuclear single quantum coherence · *INEPT*: insensitive nuclei enhanced by polarization transfer · *NOESY*: nuclear Overhauser effect spectroscopy · *TOCSY*: total correlation spectroscopy

Introduction

The PsaC subunit of Photosystem I (PS I) is a low molecular mass protein (9.3 kDa) which binds the two [4Fe-4S] clusters F_A and F_B that function as the terminal electron acceptors [1]. The remaining cofactors involved

Electronic supplementary material to this paper can be obtained by using the Springer Link server located at http://dx.doi.org/10.1007/s00775-001-0321-3.

M.L. Antonkine · D.A. Bryant · J.H. Golbeck (✉)
Department of Biochemistry and Molecular Biology,
The Pennsylvania State University,
University Park, PA 16802, USA
E-mail: jhg5@psu.edu
Tel.: +1-814-8651163
Fax: +1-814-8637024

G. Liu · D. Bentrop · I. Bertini (✉) · C. Luchinat
Magnetic Resonance Center,
Department of Chemistry,
University of Florence,
Via L. Sacconi 6,
50019 Sesto Fiorentino (Florence), Italy
E-mail: bertini@cerm.unifi.it
Tel.: +39-055-4574270
Fax: +39-055-4574271

D. Stehlik (✉)
Institut für Experimentalphysik,
Freie Universität Berlin,
Arnimallee 14, 14195 Berlin, Germany
E-mail: stehlik@physik.fu-berlin.de
Tel.: +49-30-83855069
Fax: +49-30-83856081

Present address: M.L. Antonkine
Institut für Experimentalphysik,
Freie Universität Berlin,
Arnimallee 14, 14195 Berlin, Germany

in light-induced charge separation and electron transfer from the primary donor P_{700} through the chain of acceptors A_0, A_1 to F_X are tightly bound within the membrane phase of PS I, which is composed of the large, membrane spanning, PsaA/PsaB heterodimer. PsaC is tightly bound along with two additional subunits, PsaD and PsaE, to the stromal side of PS I. The F_A and F_B centers in PsaC have the task of vectoring the electron from the interpolypeptide [4Fe-4S] center F_X, located in the stromal boundary region of the membrane phase to soluble electron carriers (ferredoxin or flavodoxin) utilized in energy-requiring metabolic processes within the cell.

Despite its essential role as an integral part of the membrane-bound PS I complex, PsaC is a highly soluble protein. This, along with its relatively low mass, allows the application of NMR techniques to determine the solution structure of the oxidized, unbound form of the protein. Attempts to obtain crystals of PsaC suitable for investigation by X-ray crystallography have not been successful (Golbeck JH, unpublished results). Given the altered properties of F_A and F_B upon binding to PS I, which are evident from EPR studies of bound versus unbound PsaC [2], important differences may be anticipated between the structures of bound and unbound PsaC. The X-ray structure of the cyanobacterial PS I complex has been modeled based on an electron density map at 4 Å resolution (PDB entry 1C51 [3]). This map includes a structural model for PsaC bound to PS I [3]. An improved structure of PS I, at an atomic resolution of 2.5 Å, is now available (PDB entry 1JB0 [4]). In this context, a solution structure suitable for comparing the bound versus unbound forms of PsaC has become a high priority and is the subject of this paper. Along with PsaD [5] and PsaE [6, 7], PsaC will be one of the few proteins whose structure is known when unbound in solution and when bound to a large membrane-protein complex. To the best of our knowledge, PsaC is the only dicluster ferredoxin-like protein to be studied in both the bound and unbound states.

The sequences of plant and bacterial PsaC are strikingly similar [8]. A lesser degree of similarity is found between PsaC and small, dicluster bacterial ferredoxins. However, both contain two [4Fe-4S] cluster binding motifs consisting of the consensus sequence CxxCxxCxxxCP, where C is cysteine, P is proline and x are other non-cysteine amino acids. Several high-resolution X-ray and NMR structures are available for the bacterial dicluster ferredoxins (PDB entries 1FDX, 1CLF, 1FDN, 2FDN, 1BLU, 1FCA, 5FD1, 1BC6, 1BQX) [9, 10, 11, 12, 13, 14, 15, 16, 17, 18] (see also reviews [19, 20]). A comparison of the NMR and X-ray structures of these ferredoxins shows that the structural details change very little between the solution and crystal phases. In PsaC, as well as in 2[4Fe-4S] ferredoxins, the iron-sulfur cluster consensus motif begins with a characteristic triplet of cysteines that ligate three irons of the first iron-sulfur center, which is equivalent to Cluster I in bacterial dicluster ferredoxins, and is referred to as F_B. It continues with a single α-helical turn that assures a well-defined distance to the fourth cysteine of the motif, which ligates one iron of the second [4Fe-4S] cluster. The second iron-sulfur center is bound to the protein in the same manner, with a triplet of cysteines from the second iron-sulfur cluster consensus motif providing ligands to the other three irons, and the fourth cysteine providing the final ligand to the first iron-sulfur center. The second iron-sulfur center in PsaC is equivalent to Cluster II in bacterial dicluster ferredoxins and is referred to as F_A. In the amino acid sequence of PsaC, cysteines 10, 13, 16 and 57 ligate Cluster I or F_B and cysteines 47, 50, 53 and 20 ligate Cluster II or F_A [28]. Both iron-sulfur cluster binding motifs and clusters themselves exhibit a local pseudo-C_2 symmetry, which applies also, but to a much lesser extent, to other regions of the protein. These central structural features are common to all dicluster ferredoxins characterized thus far, and have proven to be a good model for PsaC. This is increasingly evident from the emerging PS I X-ray structure, from the original report [21] to the most recent refinements [3, 4]. PsaC, however, differs from dicluster ferredoxins in three regions: a minor extension of the N-terminus (two residues), a sequence insertion of eight residues in the middle of the loop connecting the two consensus iron-sulfur binding motifs, and a C-terminal extension of 14 or 15 residues. These structural elements are likely to play a role for specific PsaC interactions with other components of the membrane-bound PS I complex. The amino acids in the loop insertion are considered to be involved in ferredoxin/flavodoxin binding [22, 23] and those in the C-terminus in binding of PsaC to the PsaA/PsaB core and other stromal subunits. Another significant sequence difference concerns the non-cysteine amino acids in and near the F_A and, to a lesser degree, the F_B binding motif.

Previous NMR studies of unbound PsaC have focused on the stereospecific and sequence specific assignments of the contact-shifted Hα and Hβ protons of the cysteines that ligate the [4Fe-4S] clusters, in either the fully oxidized [24] or the fully reduced [25] state of the protein. The results obtained for the oxidized state of unbound PsaC proved to be nearly identical for PsaC isolated from *Synechococcus elongatus* [24] and from *Synechococcus* sp. PCC 7002 [25], with assignments that are readily transferable between both proteins.

In this paper, we present and interpret a substantially enlarged set of NMR data that allows the solution structure of the oxidized, unbound PsaC subunit of PS I to be determined. Details of this structure are of particular interest because they are expected to deviate significantly from those of PsaC tightly bound to the PS I core. Indeed, the fact that the same protein subunit can be easily accommodated in a tightly bound, highly stable, membrane-embedded, multiprotein complex, i.e. in a predominantly hydrophobic environment, and can also comfortably take up the role of a soluble protein in aqueous solution, demands an explanation. Moreover, all results obtained thus far for highly soluble dicluster

ferredoxins and unbound PsaC indicate an equivalence of the two [4Fe-4S] clusters (F_A and F_B in PsaC), both in the oxidized and reduced state [24, 25, 26, 27]. In contrast, a distinct inequivalence between the two [4Fe-4S] clusters is observed when PsaC is bound to PS I [2, 28]. With the latter aspect in mind, we will identify and evaluate the main differences in the bound and unbound structures of PsaC and comment on their functional significance.

Materials and methods

Sample preparation

The *psa*C gene from *Synechococcus* sp. PCC 7002 was cloned and inserted in the pET-3d expression vector as described by Zhao et al. [29]. Non-labeled PsaC was overproduced in BL21 DE3 *Escherichia coli* cells grown on NCZYM media as described previously [29]. ^{15}N-enriched PsaC was obtained by growing BL21 DE3 *E. coli* cells on minimal (M9) media supplemented with ^{15}N-ammonium chloride. ApoPsaC was purified from *E. coli* as described previously [29]. The purity of the protein was verified by sodium dodecyl sulfate polyacrylamide gel electrophoresis [30].

Iron-sulfur clusters were inserted into apoPsaC in a manner similar to the published procedure [25, 31]. To 50 mL of 50 mM Tris/HCl, pH 8.3, 400 μL of 2-mercaptoethanol were added, followed by 1 mL of 5 mg/mL apoPsaC solution, 150 μL of a 60 mM iron(III) chloride solution, and 150 μL of a freshly prepared 60 mM sodium sulfide solution. All additions were performed dropwise at 20 min intervals. All solutions and Tris/HCl buffer were degassed and purged with argon prior to use. The reconstitution reaction was allowed to incubate overnight at 279 K. The solution was transferred to a controlled environment chamber (Coy, Grass Lake, Mich., USA) and all further manipulations were performed anaerobically. Solutions from 12 reconstitution reactions (a total of 60 mg of protein) were concentrated by ultrafiltration (Amicon, Beverly, Mass., USA). Excess iron and sulfide were removed by gel filtration during this procedure and the Tris buffer was substituted with 25 mM phosphate, pH 7.6 or pH 8.0. The sample was loaded onto a column packed with G-25 beads (Sigma) and the dark brown fraction was collected. A D_2O sample was prepared by concentrating the protein aqueous solution to a volume of 2 mL and by diluting it with 30 mL D_2O solution of 25 mM phosphate, pH 7.6 or pH 8.0 (uncorrected for deuterium isotope effect), followed by concentration to the original volume. The whole procedure was repeated three times. The sample was then further concentrated to a volume of 1 mL. After successful reconstitution of the [4Fe-4S] clusters, no protein precipitation was observed throughout the purification procedure. The sample (550 μL each) was aliquoted into two NMR tubes. Screw cap tubes of the highest quality available were used (catalog No. 535-TR-7 with the solid cap TR-SC-01, Wilmad Glass, Buena, NJ, USA). Since the iron-sulfur clusters decompose rapidly unless PsaC is maintained anaerobically, a strategy was developed in order to preserve anaerobic conditions through the rather lengthy NMR measurements. Unlike in the previous work [25], addition of 0.1% w/v of 2-mercaptoethanol to protect the iron-sulfur clusters was avoided, because it introduced significant problems in the interpretation of cross peaks in the diamagnetic region of the 2D NOESY and TOCSY spectra. Addition of pieces of cotton soaked in 2-mercaptoethanol between the surface of the sample and the top of the NMR tube (as described in [25]) was also avoided. Instead, the top of the NMR tube was sealed using epoxy glue prior to attaching the screw cap. This glue is a good sealing agent for anaerobic samples, because the initiator of the polymerization is a polymercaptan. Residual amounts of initiator should provide added stability to the sample in case a small amount of oxygen leaks through the screw cap. The samples were stored on ice, without freezing, inside the anaerobic chamber until use. After the initial set of measurements, we noticed that sample sealing was so effective that even when samples were stored for months outside the anaerobic chamber at 4 °C, the samples remained stable.

NMR spectroscopy

NMR spectra were acquired on Bruker AVANCE 800, AVANCE 600 and DRX 500 spectrometers operating at 800.13, 600.13 and 500.13 MHz proton Larmor frequency, respectively. The sample temperature was usually 285 K. An additional set of two-dimensional TOCSY [32] and NOESY [33] spectra at 291 K was recorded in order to resolve chemical shift degeneracies. The residual water signal was suppressed by either the superWEFT pulse sequence [34], or by presaturation, or by gradient tailored excitation (WATERGATE) [35]. The spectra were calibrated at different temperatures according to the empirical relationship $\delta_{HOD} = (-0.012T + 5.11)$ ppm, with T being the temperature in °C. ^{15}N signals were indirectly referenced to the proton frequency.

Homonuclear proton spectra (NOESY [33], TOCSY [32], clean-TOCSY [36] and DQF-COSY [37] experiments) were recorded with mixing times of 60–120 ms for the NOESY and a spin lock mixing time of 80 ms for the TOCSY spectra, respectively. The spectral window was 14.0 ppm and the recycle delay was 800 ms. Spectra consisted of 4000 data points in the f_2 and 512 increments in the f_1 dimensions with 64 transients each.

^{1}H-^{15}N HSQC [38] spectra were recorded with spectral windows of 14 ppm and 32 ppm in the ^{1}H and ^{15}N dimensions, respectively. 256 increments each with 1024 complex data points and 32 transients were collected. 3D HSQC-NOESY [39], HSQC-TOCSY [40] and HNHA [41] (to determine $^3J_{HNH\alpha}$ coupling constants) were recorded with spectral windows of 14 ppm and 32 ppm in the ^{1}H and ^{15}N dimensions, respectively. Spectra consisted of 1024 data points in the f_3, 64 increments in the f_1, and 32 increments in the f_2 dimensions with 8 transients each.

Two-dimensional spectra for the detection of connectivities between paramagnetically shifted resonances were collected using a spectral window of 40 ppm, with acquisition times on the order of 150 ms and short relaxation delays to allow for the accumulation of a high number of scans. A 20 ms TOCSY and a 10 ms NOESY spectrum with a total of 384 increments in f_1 were also recorded. Raw data were multiplied in both dimensions by a squared cosine window function and Fourier-transformed to obtain a final matrix of 1024×1024, or of 512×512 real data points for HSQC spectra. A polynomial baseline correction was applied. 1D NOE difference spectra were obtained upon selective irradiation of hyperfine-shifted, fast-relaxing signals of oxidized PsaC using previously reported methodologies [42, 43]. All NMR data were processed with the Bruker XWINNMR software. The program XEASY ([44, 45], ETH Zürich) was used for analysis of the 2D and 3D spectra.

Structure calculations

From the NOESY spectra, cross-peak intensities were determined using the elliptical integration routine implemented in XEASY and converted into proton-proton upper distance limits by the program CALIBA [46]. The program DYANA [47] employing torsion angle dynamics (TAD) combined with a simulated annealing algorithm was used to calculate a family of 400 structures starting from randomly generated conformers in 10,000 annealing steps. Several cycles of structure calculations were carried out in order to recalibrate the NOE distance constraints in an iterative manner. Stereospecific assignments of diastereotopic protons and methyl groups were obtained using the program GLOMSA [46]. Additional proton-proton upper distance limits were determined from 1D NOE difference spectra, obtained upon irradiation of the hyperfine-shifted resonances arising from Hα and Hβ protons of cysteines ligating the iron-sulfur clusters of PsaC.

$^3J_{HNH\alpha}$-derived constraints for the backbone dihedral angle φ were also applied in the structure calculations. The $^3J_{HNH\alpha}$

constants from a 3D HNHA spectrum [41] were transformed into φ dihedral angles using the Karplus relationship [48]. All dihedral angles were divided into two classes: for $^3J_{HNH\alpha}$ constants larger than 8 Hz the φ dihedral angle was restrained between –165° and –85°, while for coupling constants smaller than 4.5 Hz the angle was restrained between –80° and –30°. Thirty structures with the lowest target function values were included in the final family. The programs MOLMOL [49] and PROCHECK-NMR [50] were used for analysis of the structures.

Coordinates of the family of 30 NMR solution structures have been deposited in the Protein Data Bank (http://www.rcsb.org/pdb) under accession number 1K0T.

Results

Assignment of the NMR signals, constraint description and structure calculations

Through the use of homo- and hetereonuclear NMR spectroscopy, ^{1}H and ^{15}N resonances of 78 out of 80 amino acid residues of recombinant, oxidized PsaC were assigned. The assignment of these NMR signals, as summarized in Table S1 of the Supplementary material, is based on a combination of data, including 1D NOE, 2D NOESY, 2D TOCSY, 2D COSY, 3D HSQC-NOESY, 3D HSQC-TOCSY and HNHA experiments. Some of the experiments were specifically tailored for detection of fast-relaxing signals. Our assignment of the NMR signals is not based on any previous one or on homology to any previously described structures and is thus de novo. For some amino acids, only a partial assignment of the spin system was possible owing to a combination of signal overlap and line broadening. 1D NOE difference spectra provided essential information for the assignment of signals arising from the cysteines that ligate the two clusters (cysteines 10, 13, 16 and 57 ligate Cluster I or F_B and cysteines 47, 50, 53 and 20 ligate Cluster II or F_A), as well as for the assignment of signals of those amino acids located in the immediate vicinity of the iron-sulfur clusters (11, 12, 17, 21, 22, 48). Those signals could not be assigned based solely on the 2D and 3D spectra because the proximity of the paramagnetic metal centers causes severe line broadening through relaxation enhancement.

All structural constraints that were derived from experimental data are summarized in Table 1. Cross peaks of the 2D NOESY spectra recorded with a mixing time of 60 ms in 90% H_2O/10% D_2O solution were integrated to obtain proton-proton distances. Additional proton-proton upper distance limits were determined from 1D NOE difference spectra, obtained upon irradiation of the hyperfine-shifted resonances. The long-distance constraints obtained from 1D NOE difference spectra were especially valuable because they identify amino acids that are located close to the paramagnetic iron-sulfur centers. This information was impossible to obtain from the 2D NOESY experiment owing to the line broadening of the signals and to the failure to observe most of the protons from cysteines that ligate the iron-sulfur clusters. The proton-proton distances were calibrated with the help of the program

Table 1 Summary of NMR constraints used for DYANA structure calculation, and structural statistics for the family of 30 DYANA structures of the unbound, oxidized PsaC from *Synechococcus* sp. PCC 7002

Structural constraints	Total	Violations (in at least one structure in the final family of 30 structures)
NOESY distance constraints	1176	104
1D NOE distance constraints	111	0
Iron-sulfur cluster geometric constraints (upper and lower distance limits among iron and sulfide ions in the cubane) [51]	120	1
Hydrogen bond constraints	10	2
Overall number of meaningful (total) distance constraints[a]	1100 (1417)	107
Overall intraresidue	203	31
Overall sequential	340	24
Overall medium range	238	27
Overall long range	319	25
φ dihedral angles	6	0
χ_2 dihedral angles	8	0
Overall number of meaningful constraints	1114	107
Stereospecific assignments from GLOMSA [46]	62	–
Overall violations larger than 0.3 Å	–	0
Overall violations between 0.1 and 0.3 Å	–	107
Target function (Å^2)	0.95 ± 0.07	–
Structure analysis[b,c]		
% of residues in most favored regions and allowed regions	85.6	–
% of residues in generously allowed regions	9.1	–
% of residues in disallowed regions	5.3	–

[a]Medium-range distance constraints are those between residue i and residues $i+n$ ($2 \le n \le 5$); long-range constraints are between residue i and residues $i+m$ ($m > 5$)

[b]According to the Ramachandran plot statistic

[c]The program PROCHECK-NMR [50] was used to check the overall quality of the family of 30 DYANA structures. The entire structure, including disordered parts, was analyzed by PROCHECK-NMR. According to the criteria employed by this software, such as distribution of the backbone dihedral angles and the overall *G*-factor [50], the resolution of PsaC solution structure corresponds to a resolution of about 3 Å in X-ray crystallography

CALIBA. Figure 1a shows the number of NOEs per residue as a function of the residue number, and Fig. 1b the sequence in the one-letter code together with a schematic representation of the calibrated distance values derived from the sequential and medium-range NOEs observed in PsaC.

The angular dependence of the chemical shifts of the hyperfine-shifted resonances of the cysteines ligating F_A and F_B [24] was used to derive eight χ_2 dihedral angle constraints, all of which were given $\pm 20°$ variation range during the structure calculations. Geometric constraints arising from the virtually invariant cubane geometry of [4Fe-4S] clusters were used as described previously by Banci et al. [51] to construct the two clusters I (F_B) and II (F_A). Only six dihedral angle constraints could be derived from a 3D HNHA experiment (amino acids 33, 43, 45, 61, 67, 68). The ground state of the $[4Fe\text{-}4S]^{2+}$ clusters is diamagnetic, but a certain paramagnetic character comes about from partial population of excited paramagnetic states at room temperature. Most likely, our inability to obtain more dihedral angle constraints is due to a population of excited paramagnetic states of F_A and F_B at 285 K and the fact that in such a small protein nearly all parts except the C-terminus are affected by the magnetism of these centers. Sixty-two stereospecific assignments were obtained from the program GLOMSA. The program DYANA, employing torsion angle dynamics combined with a simulated annealing algorithm, was used to calculate the structure based on the experimental

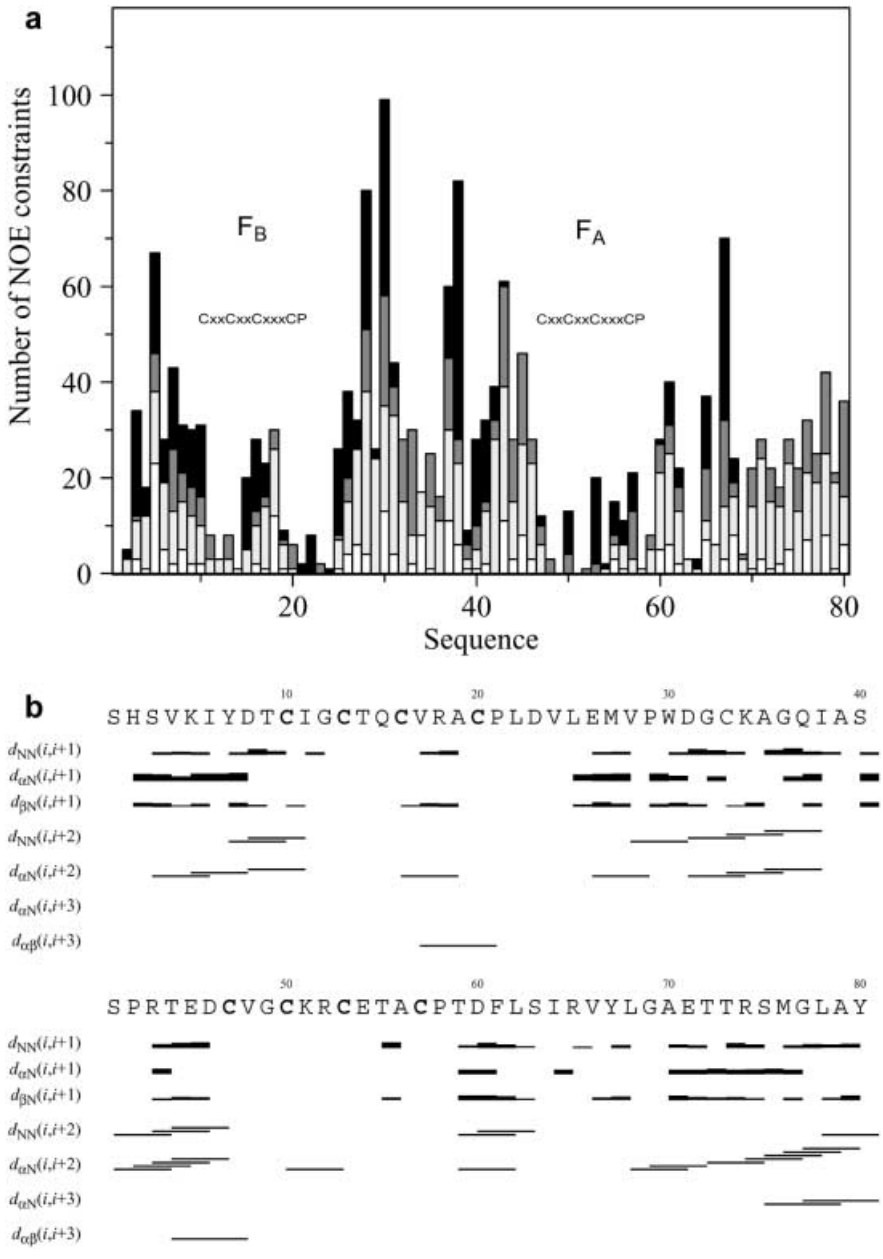

Fig. 1 **a** Distribution of the number of meaningful NOEs per residue used for structure calculations of the unbound, oxidized PsaC from *Synechococus* sp. PCC 7002. Intraresidue, sequential, medium-range and long-range NOE constraints are indicated by *white*, *light gray*, *dark gray* and *black bars*, respectively. The positions of the two consensus iron-sulfur cluster binding motifs in the sequence are indicated. **b** Schematic plot of the sequential and medium-range NOE connectivities. The *thickness* of the bar indicates the intensity of the observed cross peak. The protein sequence is given in the one-letter code. The conserved cysteines that coordinate the [4Fe-4S] clusters are indicated by *bold letters*. *d* is a calibrated distance between two protons. Note the $d_{\alpha N}$ $(i,i+2)$ and $d_{\alpha N}$ $(i,i+3)$ NOEs in the sequence stretch 68–80 which are indicative of helical secondary structure. No $d_{\alpha N}$ $(i,i+4)$ NOEs were observed

constraints. The final family contains 30 structures without consistent constraint violations and an average target function of 0.95 ± 0.07 Å^2. The RMSD from the mean structure within the family is 0.84 ± 0.15 Å for the backbone atoms and 1.35 ± 0.22 Å for all heavy atoms (calculated for a superposition of amino acids 5–67). RMSD values calculated for superpositions of different protein fragments are reported in Table 2.

The RMSD per residue values for the final DYANA family are plotted as a function of the residue number in Fig. 2. The backbone structure of PsaC in solution is depicted in Fig. 3 as a tube with a thickness proportional to the backbone RMSD. For clarity, only the backbone of residues 3–67 with RMSD values smaller than 2 Å is shown.

The final family of 30 DYANA structures was analyzed with the program PROCHECK-NMR [50]. According to the criteria employed by this software, such as distribution of backbone dihedral angles and overall "*G*-factor" [50], the resolution of the present PsaC solution structure corresponds to a resolution of about 3 Å in X-ray crystallography. This resolution is not sufficiently high to discuss specific details of the positions of side chains for most amino acids. However, as will be shown below, it is more than sufficient to demonstrate the large-scale changes in the structure between the unbound and bound forms of PsaC that emerge from this work. Therefore, the changes in the conformation of the N-terminus, pre-C-terminal region and C-terminus of PsaC described below are reliable findings, which are well outside the experimental uncertainties in the PsaC solution structure.

Description of the solution structure

The solution structure of oxidized, unbound PsaC is shown in Figs. 3 and 4, with individual structural elements of PsaC shown in Fig. 4b–e. We now describe the various elements of the secondary structure of PsaC. With the exception of the first two amino acids, the N-terminus, represented by amino acids 3–9, is structurally well defined (Figs. 3, 4a, d). The N-terminus is followed by the well-defined binding motif of the first iron-sulfur cluster in the sequence (F_B). Despite the vicinity of paramagnetic iron atoms, the F_B binding region is well defined (Figs. 3, 4a, b). Figure 4b shows the two [4Fe-4S] clusters F_B and F_A with the respective backbone of PsaC, restricted to only those amino acids that belong to the two iron-sulfur cluster binding motifs. As predicted previously, this iron-sulfur core of PsaC shows many structural features similar to those of dicluster ferredoxins (PDB entries 1FDX, 1CLF, 1FDN, 2FDN, 1BLU, 1FCA, 5FD1, 1BC6, 1BQX) [9, 10, 11,

Table 2 RMSD from the respective mean structure of the family of 30 DYANA structures, calculated for different regions of PsaC

Residue numbers	RMSD	
	Backbone	Heavy atoms
5–67	0.84 ± 0.15	1.35 ± 0.22
10–57 (two iron-sulfur binding sites and the loop connecting them)	0.69 ± 0.14	1.15 ± 0.25
22–46 (loop connecting two iron-sulfur binding sites)	0.51 ± 0.12	0.94 ± 0.16
68–80 (C-terminus)	1.87 ± 0.37	2.70 ± 0.52

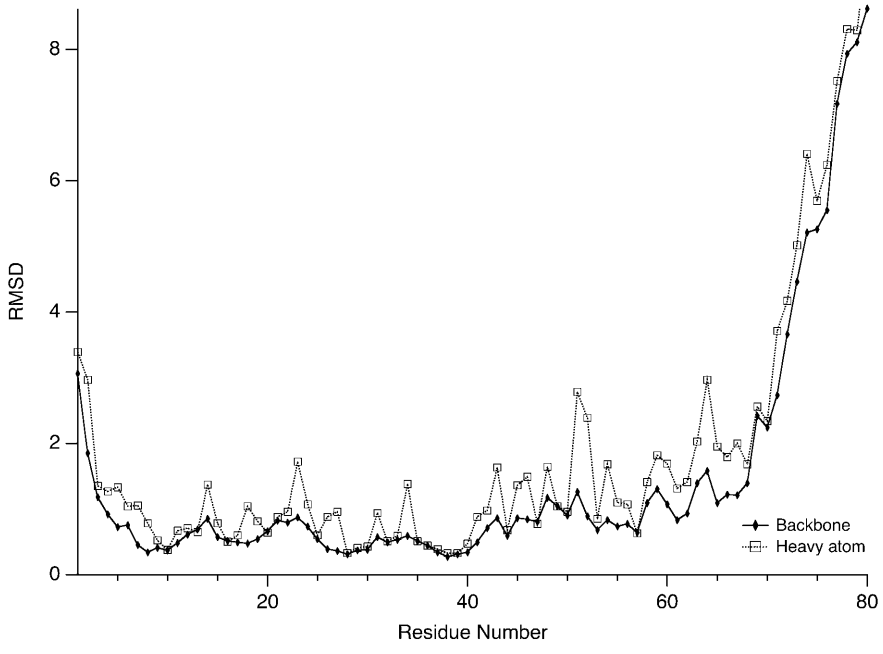

Fig. 2 Plot of global backbone (*diamonds*) and heavy atoms (*open squares*) RMSD per residue for the family of 30 DYANA structures of the unbound, oxidized PsaC from *Synechococus* sp. PCC 7002 (see also Table 2)

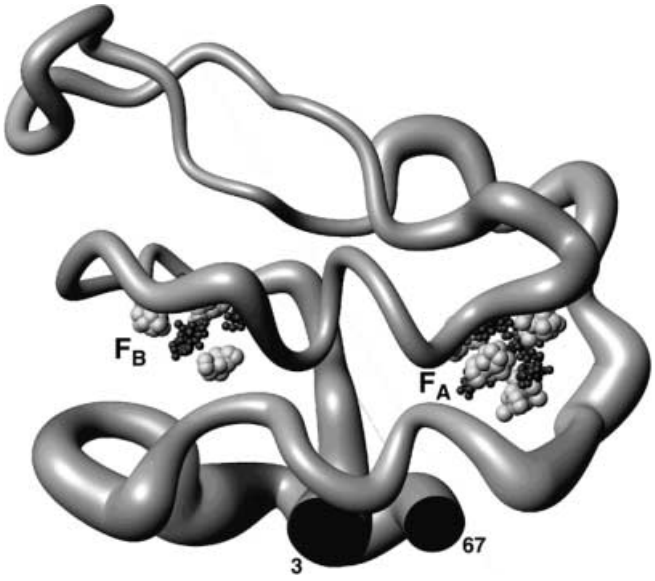

Fig. 3 "Sausage" representation of the superimposed 30 DYANA backbone structures of unbound, oxidized PsaC from *Synechococus* sp. PCC 7002. The *tube thickness* is proportional to the backbone RMSD. Only the backbone of residues 3–67, with RMSD values smaller than 2 Å (see Fig. 2), is shown. The iron and sulfide ions of the [4Fe-4S] clusters are shown for each of the 30 structures; iron atoms are shown as *dark-gray spheres*, sulfur atoms as *light-gray spheres*. Note the increased disorder of the polypeptide chain around the F_A center

12, 13, 14, 15, 16, 17, 18]. The binding sites of F_A and F_B have a fold typical of [4Fe-4S] binding sites in ferredoxins that contain one or two iron-sulfur clusters. The α-helical turn, formed by amino acids 15–19 (Figs. 3, 4a, b), connects F_B to the F_A binding site, with Cys20 being the fourth ligand to F_A. Analogous to the F_B site, the F_A site is immediately followed by an α-helical turn consisting of amino acids 52–56, with Cys57 being the fourth ligand to F_B. This feature of PsaC is similar to bacterial dicluster ferredoxins and assures a fixed distance between Cluster I (F_B) and Cluster II (F_A).

The α-helix that connects F_B to the F_A binding site is followed by an extended, structurally well-defined loop which contains a PsaC-specific sequence insertion (see Introduction) and forms two strands of an anti-parallel β-sheet connected by a turn (Fig. 4c). This structural feature is unique for PsaC, as compared to bacterial dicluster ferredoxins (PDB entries 1FDX, 1CLF, 1FDN, 2FDN, 1BLU, 1FCA, 5FD1, 1BC6, 1BQX) [9, 10, 11, 12, 13, 14, 15, 16, 17, 18]. This loop is reported to be involved in binding of ferredoxin/flavodoxin to PS I-bound PsaC [22, 23]. The secondary structure and position of the loop established here for the NMR solution structure of unbound PsaC is identical to that of PS I-bound PsaC [4].

The F_A binding site follows in the sequence. As is most apparent from Fig. 4b, a somewhat increased disorder with respect to the overall protein is observed for both the position of the F_A cluster and the surrounding polypeptide chain of the binding motif. This is particularly true when this region is compared with other, better-defined structural elements, i.e. the environment of the F_B binding site or the loop connecting the two iron-sulfur center binding sites (see above, Figs. 3, 4a–c, Table 2). Note that in the NMR structures of dicluster ferredoxins the structures of the binding motifs surrounding the iron-sulfur centers are well defined (PDB entries 1CLF, 1BC6, 1BQX [11, 17, 18]). The F_B site is also well defined in the PsaC solution structure. Therefore, relaxation effects due to the vicinity of different paramagnetic iron-sulfur clusters cannot be the cause for the disorder observed in the F_A cluster region. Rather, specific differences between the bound and unbound forms of PsaC should be investigated for possible reasons. In the dicluster clostridial ferredoxins from *C. pasteurianum* and *C. acidi urici* (PDB entries 1CLF, 2FDN) [11, 13], the binding site of the iron-sulfur Cluster II (equivalent to F_A) is in close contact with the N-terminal part of the protein. This is also true for PS I-bound PsaC, in which residues 2–5 are found close to the F_A binding site [4]. If this arrangement existed in unbound PsaC, one would expect to observe some long-range NOE connectivities between the amino acids in the N-terminal part and in the F_A binding site, but none are observed. Thus the F_A site of PsaC in solution has significantly fewer contacts with other regions of the protein than the corresponding iron-sulfur Cluster II binding site in bacterial ferredoxins [9, 10, 11, 12, 13, 14, 15, 16, 17, 18] or the same site in bound PsaC [4] (Figs. 3, 4a). This may be related to the increased disorder found in the surroundings of the F_A cluster in the solution structure.

In accordance with the increased disorder of the entire F_A region, the α-helix that follows the F_A site shows a higher degree of disorder (Figs. 3, 4a, b) in comparison to the better defined α-helix that follows the F_B site. Following the α-helical turn connecting F_A to F_B, Cys57 provides the fourth ligand to the F_B cluster. The polypeptide chain then forms a turn, which is followed by a stretch of amino acids 61–67, which we refer to as the pre-C-terminal region of PsaC. Amino acids 63–68 form a shallow loop around the N-terminal end of PsaC (Fig. 4d). If the solution structure of PsaC were similar to that of bound PsaC in the PS I complex, long-range NOE connectivities should be observed between amino acids of the N-terminus and the pre-C-terminal region on the one hand, and amino acids of the F_A binding site on the other. However, none of these expected NOE connectivities are observed in unbound PsaC. Instead, specific long-range NOE connectivities between protons of His2/Ser3 and Tyr67/Leu68 and between protons of Lys5 and Arg65/Tyr67 were observed. Figs. S1–S3 of the Supplementary material depict strips of 800 MHz 2D NOESY spectra recorded with a mixing time of 60 ms in 90% H_2O/10% D_2O which show long-range NOE connectivities between the protons of these amino acids. Specifically, NOEs are observed between 67 HN–3 Hα and 3 HN–67 Hα. Such interstrand NOEs of HN and Hα of the same residue are impossible in an anti-

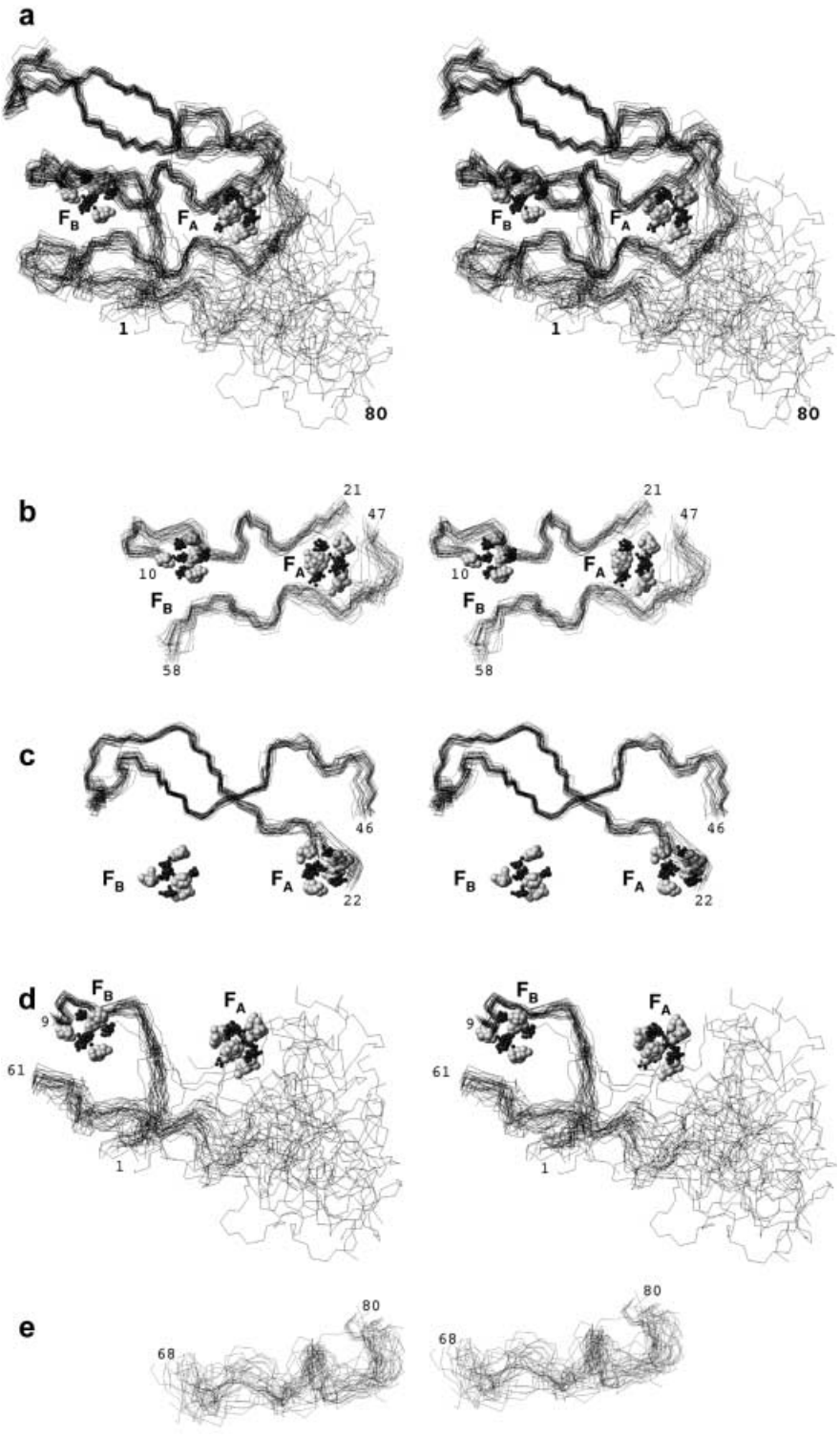

Fig. 4 **a** Backbone stereo drawing of 30 superimposed DYANA structures of unbound PsaC. The iron and sulfide ions of the [4Fe-4S] clusters of each of the 30 DYANA structures are shown with iron atoms as *dark-gray spheres*, sulfur atoms as *light-gray spheres*. The direction of the view is perpendicular to the F_A/F_B connecting axis and parallel to the stromal membrane plane of the assembled PS I complex. In **a**–**d** the family of 30 DYANA structures is shown in a superposition of amino acids 5–67. In **b**–**e**, selected structural elements of unbound PsaC are shown: **b** the two iron-sulfur clusters together with their conserved CxxCxxCxxxCP binding motifs, i.e. the backbone of amino acids 10–21 and 47–58; **c** loop region of PsaC between the two iron-sulfur binding motifs, i.e. the backbone of amino acids 22–33 in the back and 34–46 in front; **d** N-terminus (1–9), pre-C-terminal region (61–67) and disordered C-terminus (68–80); note the close contact between amino acids 2–5 and 65–68 and the position of the N-terminus between the iron-sulfur core of PsaC and the loop formed by amino acids 63–68; **e** backbone of amino acids 68–80 in the family of 30 PsaC structures is shown in superposition of solely the amino acids 68–80. The helical secondary structure of the C-terminus is clearly revealed. All figures have been prepared using MOLMOL [49]

parallel β-sheet since Hα and HN of the same residue can never be on the same side of a strand in a β-sheet. Moreover, it is not possible that both protons 3 Hα and 2 Hα give interstrand NOEs with HNs of the pre-C terminus. The Hαs of two adjacent residues on a β-strand are on opposite sides of the strand. For similar reasons, 2 Hα could not give NOEs with 68 HN and 67 HN in a β-sheet, since the HNs of neighboring residues are again on different sides of the β-strand. Therefore, this set of NOEs is not compatible with the anti-parallel β-sheet arrangement of the N-terminus and the pre-C-terminal region found for PS I-bound PsaC, but indicates a close contact between the N-terminus and the amino acids 65–68 in unbound PsaC (Fig. 4d). Thus, the solution structure shows the N-terminus positioned between the iron-sulfur core and a short loop comprising

residues 63–68 (Figs. 3, 4d). Correspondingly, as compared to the crystal structure, the N-terminus bends in solution, with a turn comprised of Val4, Lys5 and Ile6. This special cross-over arrangement of the N-terminus and pre-C-terminal region for PsaC in solution contrasts with the anti-parallel β-sheet structure established for the corresponding N- and C-terminal regions of bacterial ferredoxin structures [9, 10, 11, 12, 13, 14, 15, 16, 17, 18] and with the anti-parallel β-sheet arrangement of the N-terminus and pre-C-terminal region in PsaC bound to PS I (β-sheets β_{1A} and β_{4A} in PDB entry 1JB0) [4].

Finally, amino acids 68–80 of the C-terminus of PsaC form a disordered helix-like structure that does not have any packing interactions with the rest of the protein. This is already apparent from Fig. 1a, which shows that amino acids 69–80 lack any long-range NOE distance constraints. On the other hand, superposition of just the residues 68–80 within the family of 30 DYANA structures readily reveals the helical secondary structure of the PsaC C-terminus (Fig. 4e). This is in agreement with the significant number of medium-range NOEs found in that region (Fig. 1a). For example, the $d_{\alpha N}$ $(i,i+2)$ and $d_{\alpha N}$ $(i,i+3)$ NOEs, indicative of helical secondary structure, are observed for amino acids 68–80. The C-terminus of PsaC is the only part of the protein that is apparently quite distant from the iron-sulfur clusters and is therefore unlikely to be influenced by their paramagnetism. It is conceivable that the C-terminus of unbound PsaC has an intrinsically higher mobility compared with other parts of the protein (e.g. the loop connecting the two iron-sulfur binding sites). This is suggested by the absence of a continuous series of $^3J_{HNH\alpha}$ coupling constants below 4.5 Hz, and the total absence of $d_{\alpha\beta}$ $(i,i+3)$ and $d_{\alpha N}$ $(i,i+4)$ NOEs typical for α-helices. However, while the C-terminus may not have a stable conformation, it must have a definite helical propensity leading to the observed medium-range NOEs (Fig. 1a, b). The population of helical conformations for a significant fraction of the time can also be deduced from the upfield shifts of Hα protons belonging to residues 69–79 with respect to random coil chemical shifts [52]. In PsaC there is an average upfield shift of 0.04 ± 0.02 ppm observed for the Hα protons of residues 69–79; the threshold value of the chemical shift index that would indicate a stable helix is an upfield shift of more than 0.1 ppm [53].

In summary, the PsaC solution structure is characterized by the following structural elements. The well-defined regions include the N-terminus (except for the first two amino acids), the [4Fe-4S] cluster F_B binding site (with the Fe and S atoms and the surrounding cysteine binding motif), the α-helix following the F_B binding site, and the loop connecting the iron-sulfur cluster binding motifs forming two strands of an anti-parallel β-sheet connected by a turn. A larger disorder is found for the subsequent F_A binding site, which is also associated with a distortion of the α-helical turn following the F_A site. Finally, the C-terminal extension of PsaC forms a disordered helix-like structure.

Discussion

Most bacterial dicluster ferredoxins with available X-ray crystal and NMR solution structures show high similarity between both types of structures and, in general, a high similarity of the overall three-dimensional structures is observed for this class of proteins (PDB entries 1FDX, 1CLF, 1FDN, 2FDN, 1BLU, 1FCA, 5FD1, 1BC6, 1BQX) [9, 10, 11, 12, 13, 14, 15, 16, 17, 18] (see also reviews [19, 20]). In contrast, some of the most prominent features of the NMR solution structure of PsaC stand out as clearly different when compared with the X-ray structure of the PsaC subunit bound within the fully assembled membrane-bound PS I complex (PDB entry 1JB0 [4]). These differences will now be compared and discussed.

The C-terminus of PsaC is disordered, although it has a helical secondary structure. In the Results section we present arguments that indicate the intrinsic mobility of the C-terminal region in solution. In the absence of contacts with the PsaA/PsaB/PsaD/PsaE polypeptides the solution structure shows that the C-terminus is not in an extended coil conformation but rather has a high helical propensity (Fig. 4e). In contrast, no secondary structural elements are reported for the C-terminal extension (68–80) of bound PsaC in the PS I complex [4]. The C-terminus of PsaC in fully assembled PS I is located in the binding interface between the PsaD and PsaA polypeptides [4]; consequently, the high degree of structural flexibility of the C-terminus found in unbound PsaC is altered to a fixed and extended structure in the PS I-bound form of the protein. During assembly this requires unwinding of the helical structure of the C-terminal end (68–80) found in solution.

In the X-ray structure of PS I, parts of the N-terminus (3–7) and of the pre-C-terminal region (64–67) of PsaC form an anti-parallel β-sheet structure (β-sheets β_{1A} and β_{4A} in PDB entry 1JB0), and are positioned close to the F_A site [4]. A sequence alignment between PsaC and clostridial ferredoxins shows that the pre-C-terminal region of PsaC is equivalent to the C-terminus of bacterial ferredoxins (see Fig. 1 in Antonkine et al. [25]). The anti-parallel arrangement of the N-terminus and pre-C-terminal region of bound PsaC is in good agreement with the two-stranded anti-parallel β-sheet arrangement that is typical for the N- and C-termini of bacterial ferredoxins [9, 10, 11, 12, 13, 14, 15, 16, 17, 18]. In sharp contrast, the N- and pre-C-termini in the structure of unbound PsaC in solution are neither parallel nor close to the F_A site. Instead, the N-terminus bends, and thus the anti-parallel β-sheet arrangement of the N-terminus and pre-C-terminal region of bound PsaC in PS I is broken up in solution. Therefore, the N-terminus and pre-C-terminal regions will have to undergo structural rearrangements during the transition from unbound PsaC in solution to bound PsaC in the fully assembled PS I complex.

Another special feature of the solution structure is the increased disorder found for the F_A binding region as compared to the F_B binding region (Fig. 4b). This correlates with the fact that the F_A site in the PsaC solution structure has significantly fewer contacts with other regions of the protein than the corresponding iron-sulfur Cluster II binding site in bacterial ferredoxins [11, 13] or the same site in bound PsaC [4] (see Results). Increased solvent interaction could also contribute to the increased disorder found for the F_A binding site of PsaC in solution. For example, in the dicluster clostridial ferredoxins from *C. pasteurianum* and *C. acidi urici* (PDB entries 1CLF, 2FDN) [11, 13] the binding site of the iron-sulfur Cluster II (equivalent to F_A) is protected from interaction with the solvent by the N-terminus, which is in close contact with it. As mentioned above, this is not the case for PsaC in solution.

In summary, formation of a disordered and curled-up helical structure on the C-terminus of PsaC, and a displacement of the N-terminus and pre-C-terminal region of PsaC away from the F_A binding site, accompanied by bending of the N-terminus, are structural features of unbound PsaC in solution which are distinctly different from PsaC bound within the PS I complex.

The question arises as to what is a possible driving force for the unusual structural features observed in the PsaC solution structure. From sequence analysis it had already been noted (see Scheme 2 in Kamlowski et al. [21]) that the F_A binding site in PsaC differs significantly in its non-cysteine amino acid composition from the F_B site and from the corresponding binding sites in bacterial mono- and dicluster [4Fe-4S] ferredoxins. In particular, a significantly larger number of charged amino acids are found within and preceding the F_A binding motif. This information should be combined and correlated with the recently confirmed finding that in bound PsaC the F_A cluster is proximal to the F_X cluster [3, 4, 28, 54, 55, 56, 57, 58] which is located within the stroma-facing central part of the PsaA/PsaB polypeptide core. As a consequence, the F_A binding site in bound PsaC must be closely packed into the interface between the PsaA/PsaB core and the stromal PsaD/PsaC/PsaE complex. The charged amino acids specific to the surroundings of the F_A site can be expected to be of critical importance for the binding contacts to these polypeptides. Indeed, the recently published structure of PS I at 2.5 Å resolution fully confirms this expectation [4]. A detailed analysis of these contacts and of the consequences for the assembly of PS I is now in progress. In unbound PsaC, however, all charged amino acids involved in interpeptide contacts will be freed and may add to a stronger solvent interaction. Interestingly, this can provide an additional reason for the high solubility of unbound PsaC, a feature which is not expected for a protein designed to be tightly bound within a membrane-bound and multi-subunit protein complex. In particular, the pair of neighboring equally (positively) charged amino acids Lys51 and Arg52, located between the second and third cysteine of the F_A binding motif, stands out as a candidate for critical contacts of bound PsaC by ionic interaction to the PsaA/PsaB heterodimer core. Moreover, the F_A binding motif is preceded by a pair of equally (negatively) charged amino acids (Glu45, Asp46). From their positions in the sequence, the latter amino acids are likely to be involved in critical contacts within the multiprotein complex composed of PsaC/PsaD/PsaE. Another pair of equally (positively) charged amino acids (Lys5 and Arg65) may be of interest in this context because they are in close spatial contact in the middle of the anti-parallel β-sheet arrangement characteristic for bound PsaC. All these charged amino acids are located close to interpeptide surfaces and, therefore, likely to be involved in contacts. In solution, these amino acids are freed from their contacts and may add to the repulsive force experienced by the more hydrophobic pre-C-terminal region of PsaC, which interacts much more closely with the F_A site in the bound form.

The emerging special structural features of unbound PsaC are very likely associated with other unusual biochemical and biophysical properties of this protein. Within the PS I complex, bound PsaC is surprisingly stable under aerobic conditions and the F_A/F_B iron-sulfur centers remain intact up to relatively high temperatures. In an aerobic environment the half-inactivation occurs at 70 °C in a PS I preparation of *Synechococcus elongatus* [59], at 60 °C in pea thylakoid membranes [60] (incubation times in both studies were 5 min) and at 53 °C in spinach thylakoid membranes [61]. Thus, even in mesophilic organisms, PS I-bound PsaC is thermostable. In contrast, unbound PsaC is particularly unstable and must be handled under strictly anaerobic conditions, usually at temperatures below 18 °C [25, 31]. Note that the thermostability of PsaC isolated from the thermophile *Synechococcus elongatus* is significantly higher than that of PsaC isolated from the mesophile *Synechococcus* sp. PCC 7002; however, the protein still has to be maintained under strictly anaerobic conditions. This increase in thermostability allowed Bentrop et al. [24] to record NMR data at 37 °C, far above what is possible for the PsaC reported in this paper. In general, protein-bound [4Fe-4S] clusters have been noted to be shielded from direct interactions with solvent by a number of hydrophobic amino acids [12, 14, 19, 20, 62, 63] or by contacts with other domains of the protein, similar to the case of clostridial dicluster ferredoxins from *C. pasteurianum* and *C. acidi urici* [11, 13]. In the case of unbound PsaC, however, the conformational changes in comparison to bound PsaC – mainly the concerted movement of N-terminal and pre-C-terminal regions away from the F_A site – will leave the F_A cluster more accessible to solvent and hence much less stable. The process of degradation of PsaC is likely to proceed initially through the oxidation of the bridging sulfide atoms by molecular oxygen, resulting in the loss of the iron atoms and the formation of cysteine-bound zero-valence sulfur [64, 65].

The EPR spectra of the reduced F_A and F_B iron-sulfur clusters undergo large changes upon binding of PsaC to P700-F_X cores in the absence of PsaD and PsaE. These involve sharpening of the linewidths and a change in characteristic *g*-values of the EPR signals of F_A and F_B [2]. As we show by comparing the PsaC solution structure with the 2.5 Å crystal structure of PS I [4], these changes are most likely a result of the large conformational changes of the N-terminal, pre C-terminal and C-terminal regions of PsaC. Specifically, this is due to the formation of a disordered helix at the C-terminus and the concerted movement of the N-terminus and pre-C-terminal region away from the F_A site in unbound PsaC. A detailed discussion of the changes in the EPR spectra, in connection with a comprehensive comparison of the bound and unbound forms of PsaC will be reported in a forthcoming publication.

A final comment arises from the previous finding that the PsaD and PsaE subunits do not assemble onto PS I in a *psa*C null mutant [66]. Note that, when over-expressed in *E. coli* and individually purified, the recombinant PsaC, PsaD and PsaE proteins do not bind to each other in solution; thus they do not form any initial "pre-complex" in solution in the absence of the PS I core polypeptides (as determined by high-performance liquid chromatography; Golbeck JH, unpublished results). This should be combined with the observation that the EPR linewidths of F_A and F_B sharpen and the principal *g*-tensor values change upon binding of PsaC to the P700-F_X core. A further sharpening of the linewidth as well as adjustment of the *g*-tensor to that established for F_A and F_B in fully assembled PS I are observed after PsaD binds [2]. Therefore, the assembly of the stromal PS I subunits is likely to occur stepwise: first, PsaC binds to the P700-F_X core, then PsaD and PsaE bind. The observed structural differences between bound and unbound PsaC are expected to be important for the assembly mechanism. We suggest that the conformational changes occurring in PsaC upon binding to PS I act as a switch for subsequent binding of the PsaD and PsaE polypeptides. Thereby the PS I assembly process is completed and the magnetic properties of F_A and F_B specific to the fully assembled PS I complex are established.

Acknowledgements This work was supported by the European Union, Large-Scale Facility grant ERBCHGECT950033 to the Florence laboratory, by National Science Foundation grants to J.H.G. (MCB-9723661 and MCB-0117079) and to D.A.B (MCB-9723469), and by the DFG under SFB 498, A3 (D.S.). We thank Dr. Gaozhong Shen for his contribution in the early stages of the project.

References

1. Golbeck JH (1994) In: Bryant DA (ed) The molecular biology of cyanobacteria. Kluwer, Dordrecht, The Netherlands, pp 179–220
2. Li N, Zhao J, Warren PV, Warden JT, Bryant DA, Golbeck JH (1991) Biochemistry 30:7863–7872
3. Klukas O, Schubert WD, Jordan P, Krauss N, Fromme P, Witt HT, Saenger W (1999) J Biol Chem 274:7351–7360
4. Jordan P, Fromme P, Witt HT, Klukas O, Saenger W, Krauss N, (2001) Nature 411:909–917
5. Xia ZC, Broadhurst RW, Laue ED, Bryant DA, Golbeck JH, Bendall DS (1998) Eur J Biochem 255:309–316
6. Falzone CJ, Kao YH, Zhao JD, Bryant DA, Lecomte JTJ (1994) Biochemistry 33:6052–6062
7. Mayer KL, Shen GZ, Bryant DA, Lecomte JTJ, Falzone CJ (1999) Biochemistry 38:13736–13746
8. Golbeck JH, Bryant DA (1991) Curr Top Bioenerg 16:83–177
9. Adman ET, Sieker LC, Jensen LH (1973) J Biol Chem 248:3987–3996
10. Adman ET, Siefker LC, Jensen LH (1976) J Biol Chem 251:3801–3806
11. Bertini I, Donaire A, Feinberg BA, Luchinat C, Piccioli M, Yuan HP (1995) Eur J Biochem 232:192–205
12. Duee ED, Fanchon E, Vicat J, Sieker LC, Meyer J, Moulis JM (1994) J Mol Biol 243:683–695
13. Dauter Z, Wilson KS, Sieker LC, Meyer J, Moulis JM (1997) Biochemistry 36:16065–16073
14. Moulis JM, Sieker LC, Wilson KS, Dauter Z (1996) Protein Sci 5:1765–1775
15. Tranqui D, Jesior JC (1995) Acta Crystallogr Sect D 51:155–159
16. Stout CD (1993) J Biol Chem 268:25920–25927
17. Aono S, Bentrop D, Bertini I, Donaire A, Luchinat C, Niikura Y, Rosato A (1998) Biochemistry 37:9812–9826
18. Aono S, Bentrop D, Bertini I, Cosenza G, Luchinat C (1998) Eur J Biochem 258:502–514
19. Sticht H, Rosch P (1998) Prog Biophys Mol Biol 70:95–136
20. Bentrop D, Capozzi F, Luchinat C (2001) In: Bertini I, Sigel A, Sigel H (eds) Handbook on metalloproteins. Dekker, New York, pp. 357–460
21. Kamlowski A, van der Est A, Fromme P, Krauss N, Schubert WD, Klukas O, Stehlik D (1997) Biochim Biophys Acta 1319:199–213
22. Fischer N, Hippler M, Setif P, Jacquot JP, Rochaix JD (1998) EMBO J 17:849–858
23. Fischer N, Setif P, Rochaix JD (1999) J Biol Chem 274:23333–23340
24. Bentrop D, Bertini I, Luchinat C, Nitschke W, Muhlenhoff U (1997) Biochemistry 36:13629–13637
25. Antonkine ML, Bentrop D, Bertini I, Luchinat C, Shen G, Bryant DA, Stehlik D, Golbeck JH (2000) J Biol Inorg Chem 5:381–392
26. Malkin R, Aparicio PJ, Arnon DI (1974) Proc Natl Acad Sci USA 71:2362–2366
27. Wynn RM, Malkin R (1988) FEBS Lett 229:293–297
28. Golbeck JH (1999) Photosynth Res 61:107–144
29. Zhao J, Warren PV, Li N, Bryant DA, Golbeck JH (1990) FEBS Lett 276:175–180
30. Laemmli UK (1970) Nature 227:680–685
31. Mehari T, Parrett KG, Warren PV, Golbeck JH (1991) Biochim Biophys Acta 1056:139–148
32. Bax A, Davis DG (1985) J Magn Reson 65:355–360
33. Wider G, Macura S, Kumar A, Ernst RR, Wüthrich K (1984) J Magn Reson 56:207–234
34. Inubushi T, Becker ED (1983) J Magn Reson 51:128–133
35. Sklenar V, Piotto M, Leppik R, Saudek V (1993) J Magn Reson Ser A 102:241–245
36. Griesinger C, Otting G, Wuethrich K, Ernst RR (1988) J Am Chem Soc 110:7870–7872
37. Rance M, Sörensen OW, Bodenhausen G, Wagner G, Ernst RR, Wüthrich K (1983) Biochem Biophys Res Commun 117:479–485
38. Bodenhausen G, Ruben DJ (1980) Chem Phys Lett 69:185–189
39. Marion D, Driscoll PC, Kay LE, Torchia DA, Wingfield PT, Bax A, Gronenborn AM, Clore GM (1989) Biochemistry 28:6150–6156
40. Marion D, Kay LE, Torchia DA, Bax A (1989) J Am Chem Soc 111:1515–1517

41. Vuister GW, Bax A (1993) J Am Chem Soc 115:7772–7777
42. Banci L, Bertini I, Luchinat C, Piccioli M, Scozzafava A, Turano P (1989) Inorg Chem 28:4650–4656
43. Johnson RD, Ramaprasad S, La Mar GN (1983) J Am Chem Soc 105:7205–7206
44. Eccles C, Güntert P, Billeter M, Wüthrich K (1991) J Biomol NMR 1:111–130
45. Bartels C, Xia TH, Billeter M, Güntert P, Wüthrich K (1995) J Biomol NMR 5:1–10
46. Güntert P, Braun W, Wüthrich K (1991) J Mol Biol 217:517–530
47. Güntert P, Mumenthaler C, Wüthrich K (1997) J Mol Biol 273:283–298
48. Pardi A, Billeter M, Wüthrich K (1984) J Mol Biol 180:741–751
49. Koradi R, Billeter M, Wüthrich K (1996) J Mol Graph. 14:51–55
50. Laskowski RA, Rullmannn JA, MacArthur MW, Kaptein R, Thornton JM (1996) J Biomol NMR 8:477–486
51. Banci L, Bertini I, Eltis LD, Felli IC, Kastrau DHW, Luchinat C, Piccioli M, Pierattelli R, Smith M (1994) Eur J Biochem 225:715–725
52. Wüthrich K (1986) NMR of proteins and nucleic acids. Wiley, New York
53. Wishart DS, Sykes BD, Richards FM (1992) Biochemistry 31:1647–1651
54. Vassiliev IR, Jung YS, Yang F, Golbeck JH (1998) Biophys J 74:2029–2035
55. Mamedov MD, Gourovskaya KN, Vassiliev IR, Golbeck JH, Semenov AY (1998) FEBS Lett 431:219–223
56. Diaz-Quintana A, Leibl W, Bottin H, Setif P (1998) Biochemistry 37:3429–3439
57. Lakshmi KV, Jung YS, Golbeck JH, Brudvig GW (1999) Biochemistry 38:13210–13215
58. Shinkarev VP, Vassiliev IR, Golbeck JH (2000) Biophys J 78:363–372
59. Sonoike K, Hatanaka H, Katoh S, Itoh S (1990) Plant Cell Physiol 31:865–870
60. Shuvalov VA (1976) Biochim Biophys Acta 430:113–121
61. Hoshina S, Sakurai R, Kunishima N, Wada K, Itoh S (1989) Biochim Biophys Acta 1015:61–68
62. Fukuyama K, Nagahara Y, Tsuikihara T, Katsube Y, Hase T, Matsubara H (1988) J Mol Biol 199:183–193
63. Fukuyama K, Matsubara H, Tsuikihara T, Katsube Y (1989) J Mol Biol 210:383–398
64. Petering D, Fee JA, Palmer G (1971) J Biol Chem 246:643–653
65. Golbeck JH, Lien S, San Pietro A (1977) Arch Biochem Biophys 178:140–150
66. Yu JP, Smart LB, Jung YS, Golbeck J, Mcintosh L (1995) Plant Mol Biol 29:331–342